2.3 IRRADIATION-DAMAGE BEHAVIOR IN ADVANCED STEELS - C. M. Parish, Y. Katoh (Oak Ridge National Laboratory) and S. Kondo (Kyoto University, Japan)

OBJECTIVE

Determine the irradiation response of the newly developed 9Cr-based ODS/NFA (oxide dispersion strengthened / nanostructured ferritic alloy) steels and compare to F82H.

SUMMARY

A 650°C heavy-ion irradiation was performed on 9YWTV, a new 9Cr NFA. This was compared to F82H as a baseline material. Advanced TEM (transmission electron microscopy)-based methods were used to characterize the irradiated zone, and compare to the unirradiated base material. Broadly speaking, little residual radiation damage in the form of black spots or dislocation loops was observed in either the 9YWTV or F82H material, even at areas of the highest dose (>100 dpa). This is likely a result of the high irradiation temperature causing rapid annealing of the irradiation-induced damage. Elemental mapping using EDS (X-ray energy dispersive spectroscopy) or EFTEM (energy filtered TEM) showed evolution of the fine-scale precipitates.

PROGRESS AND STATUS

Introduction

As a screening experiment to begin understanding 9Cr NFA irradiation effects, a high-dose 650°C irradiation was performed at the Kyoto University DuET facility. Both 9YWTV NFA and F82H RAFM alloy were irradiated. Advanced characterization was used with the intent of analyzing the changes to the microstructure driven by the irradiation, and using the unirradiated material below the ion range as an internal control specimen for comparison of irradiated and unirradiated microstructures. This is intended to begin providing microstructural insight to the irradiation-driven mechanisms that will dominate for fission irradiation tests and possible eventual fusion service.

Experimental Procedure

9YWTV-PM1 material [1] (Fe–9Cr–2W–0.4Ti–0.2V–0.12C–0.3Y_2O_3) and F82H material were subjected to heavy-ion irradiation (6.4 MeV Fe, 1.5×10^{21} ions/m^2, ~150 dpa peak, ~2 μm range) at 650°C, using the DuET facility at Kyoto University. Calculations for dpa used Stoller's method [2]. Scanning TEM (STEM) based methods, particularly imaging and high-efficiency EDS mapping, were performed at the North Carolina State University Analytical Instrumentation Facility (NCSU AIF) using the probe-corrected FEI Titan G2 with ChemiSTEM instrument operated at 200 keV. Analysis of the EDS spectrum images (SIs) used the Sandia National Laboratory AXSIA computer code [3].

Results

Interestingly, low-angle annular dark field (LAADF) imaging in aberration-corrected STEM provides excellent diffraction contrast and well complements the standard bright field (BF) and high-angle annular dark field (HAADF) images. Although significant defect densities (dislocations, small spots) are observed, no gross differences are present between the irradiated and unirradiated regions; Figure 1 illustrates that although defects are visible in BF mode (i.e., red arrows), higher contrast on many of the defects (such as grain boundaries) are present in LAADF mode than in either BF or HAADF. High densities of defects are present in both the irradiated and unirradiated regions (blue and green arrows), indicative of little residual damage in the forms commonly observed at lower irradiation temperatures. (The ultrafine grain sizes

prevent tilting to clear diffraction conditions, so conventional two-beam TEM of defect strain centers is not feasible.) Precipitates, particularly in the F82H, are most easily seen in LAADF mode.

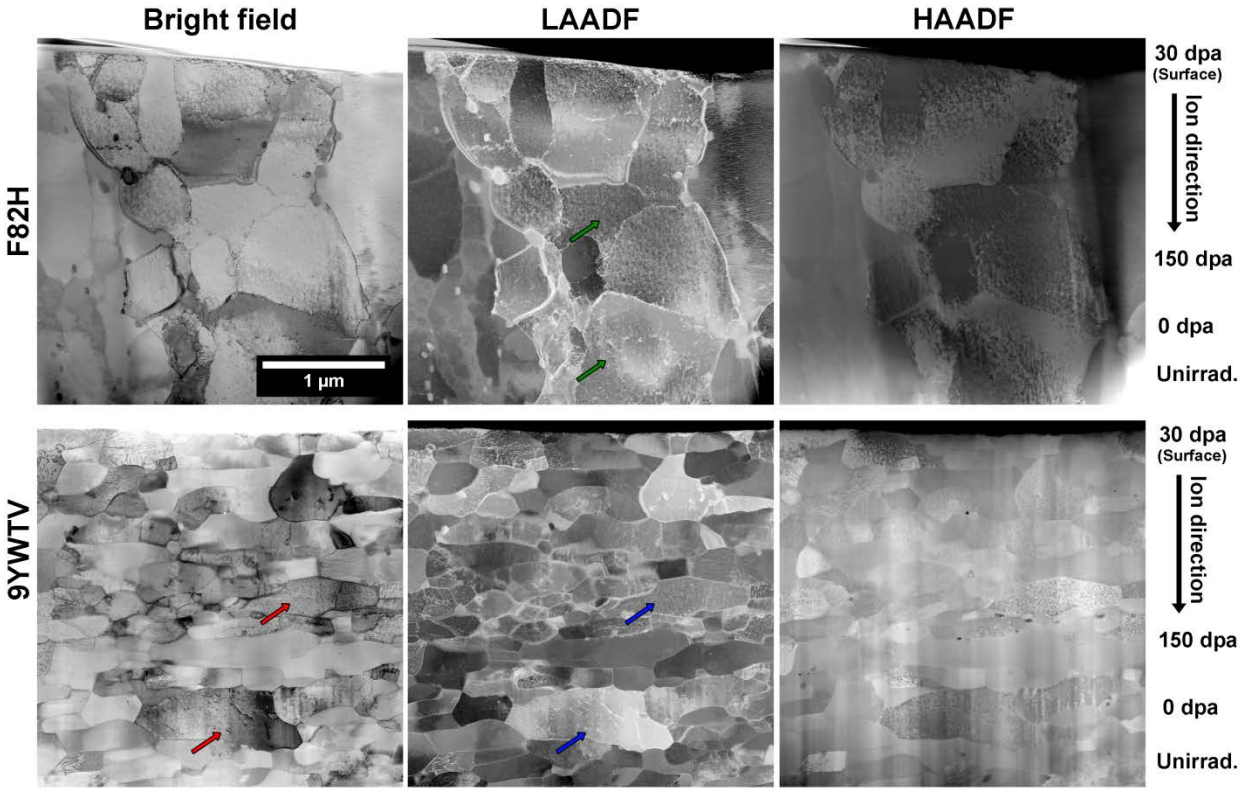

Figure 1. STEM imaging of 650°C, 150 dpa ion-irradiated F82H and 9YWTV. LAADF, low-angle annular dark field. HAADF, high-angle annular dark field.

High-efficiency X-ray mapping indicated multiple populations of precipitates in both alloys; Figure 2 (low magnification, mapping the entire depth of the bombarding particle [4]) where no appreciable differences are visible between the irradiated (shallow) and unirradiated (deep) regions in terms of precipitates present. Additionally, no radiation-induced segregation (RIS) was observed, Figure 3, which is unsurprising at 650°C but experimental confirmation provides greater confidence in material robustness at this temperature.

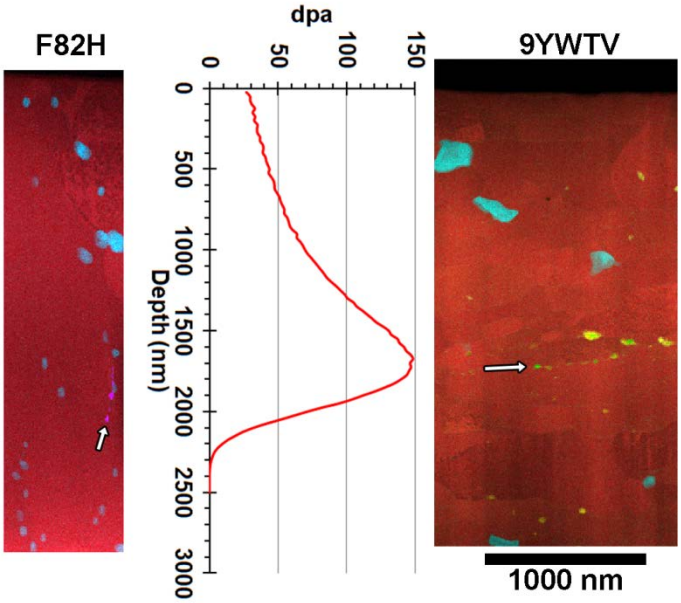

Figure 2. Multivariate statistical analysis (MVSA) decompositions of X-ray spectrum images 650°C-irradiated specimens. Chart shows SRIM-calculated dpa. Colors indicate the identity of the precipitates. Both specimens: red, Fe-Cr matrix; cyan, Cr-W-carbides. F82H only: magenta (arrowed) V-Ta-carbides. 9YWTV only: Yellow, Ti-Cr-carbides; green: Al-Ti-oxides (arrowed).

Higher magnification maps of F82H (Figure 3, depth ~1000 nm, ~50 dpa) shows no measurable radiation induced segregation (albeit along an inclined boundary, but inclined boundaries in NFA 14YWT with appreciable processing-induced segregation have been measured using the technique [5]).

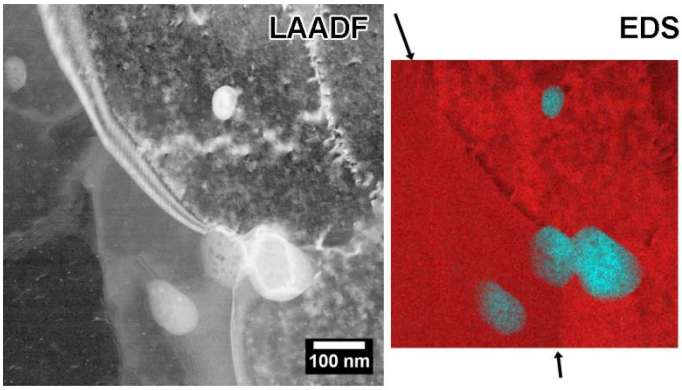

Figure 3. Low-angle annular dark field (LAADF) STEM image and multivariate statistical analysis decomposition of the EDS spectrum image. Red is the Fe-Cr matrix and cyan the Cr-W(-V) rich carbides. Arrows denote a grain boundary; no statistically significant RIS was detected. 650°C, ~50 dpa.

In the 9YWTV NFA material, irradiation was observed to result in a coarser population of the Ti-Y nanoclusters (NCs) that are believed to provide NFAs high creep and irradiation resistance.

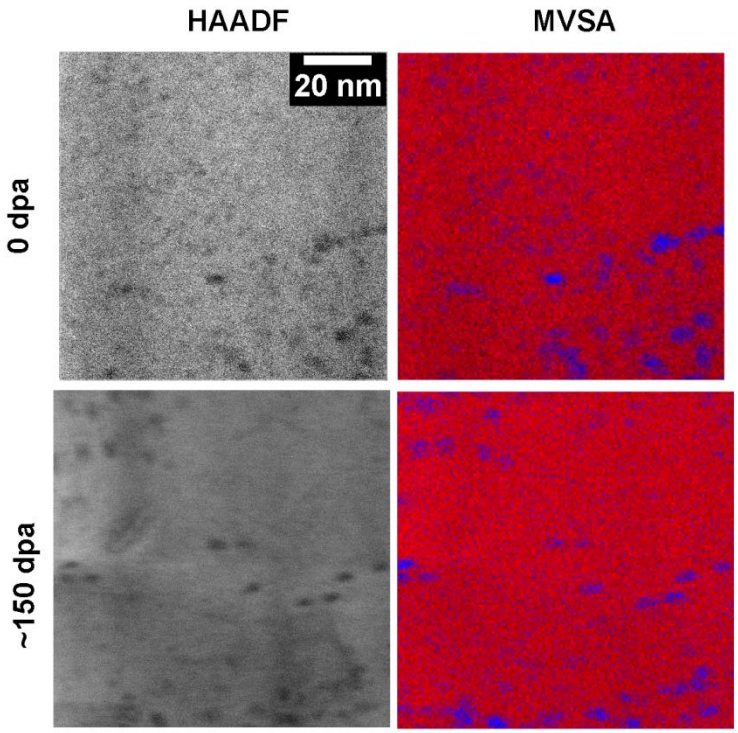

Figure 4. 9YWTV NFA irradiated at 650°C. High-angle annular dark field (HAADF) STEM shows finer precipiates in the unirradiated region than in the irradiated. MVSA decompositions (red: Fe-Cr-W matrix, blue: Y-Ti-O nanoclusters) shows the precipitates visible in HAADF are the nanoclusters.

The lack of large RIS in either material is mostly attributable to the high temperature (650°C). The carbides in the F82H showed damage, however, at higher dose regions (visible in Figure 3, but more clearly in Figure 5) in which the carbides were appearing to fracture or fragment; in unirradiated or lightly-irradiated (deep) areas, this was not observed (Figure 6). This could indicate, at least at this temperature and at the rather high dose rates used in ion irradiation, that the carbides are slowly damaged by the irradiation. (More statistics are needed, however, before this observation can be conclusive.) The NCs in the NFA (Figure 4 above), conversely, although coarsening slightly, maintain their identity (at least to the resolution of STEM-EDS of particles embedded in a matrix foil). This may indicate the NFA will be more stable against high-temperature irradiation at high dose levels.

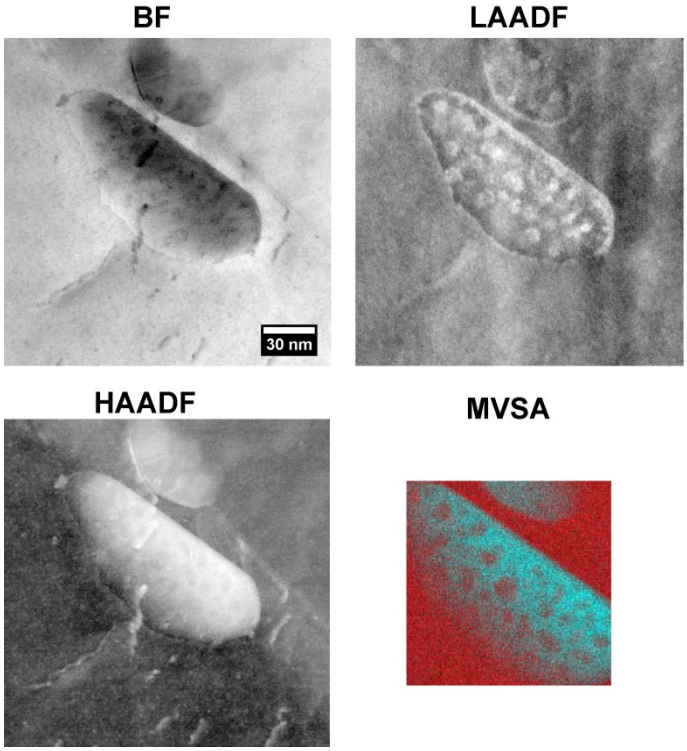

Figure 5. STEM images and MVSA decomposition of EDS data for carbides in F82H. Depth ~700 nm, dose ~50 dpa, 650°C. The carbides appear to be breaking up of fragmenting. MVSA: Red, Fe-Cr matrix, cyan, Cr-W-V(-Ta) carbide.

These results imply good microstructural stability of F82H, and very good stability of 9YWTV, to high-dose heavy-ion irradiation at 650°C. They also illustrate the importance of using the latest generation of analytical electron microscope in order to fully characterize the microstructure. Short-term follow-on work will involve helium+heavy ion irradiations to begin measuring the helium mitigation effects in 9YWTV, and future work involving neutron irradiation may be promising.

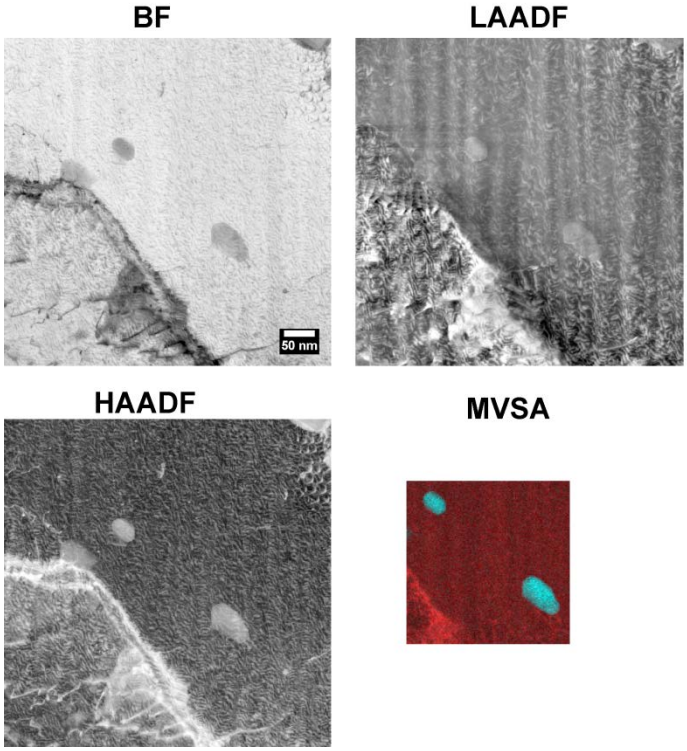

Figure 6. STEM images and MVSA decomposition of EDS data for carbides in F82H. Depth ~2300 nm, dose 0~10 dpa, 650°C. The carbides appear not to be breaking up of fragmenting. MVSA: Red, Fe-Cr matrix, cyan, Cr-W-V(-Ta) carbide.

Acknowledgements

9YWTV material provided by Dr. T. S. Byun. NCSU Titan TEM: We acknowledge the use of the Analytical Instrumentation Facility (AIF) at North Carolina State University, which is supported by the State of North Carolina and the National Science Foundation.

References

[1] T.S. Byun, J.H. Yoon, D.T. Hoelzer, Y.B. Lee, S.H. Kang, S.A. Maloy, Process development for 9Cr nanostructured ferritic alloy (NFA) with high fracture toughness, Journal of Nuclear Materials, 449 (2014) 290-299.

[2] R.E. Stoller, M.B. Toloczko, G.S. Was, A.G. Certain, S. Dwaraknath, F.A. Garner, On the use of SRIM for computing radiation damage exposure, Nuclear Instruments & Methods in Physics Research Section B-Beam Interactions with Materials and Atoms, 310 (2013) 75-80.

[3] P.G. Kotula, M.R. Keenan, J.R. Michael, Automated analysis of SEM X-ray spectral images: a powerful new microanalysis tool, Microscopy and Microanalysis, 9 (2003) 1-17.

[4] C.M. Parish, R.M. White, J.M. LeBeau, M.K. Miller, Response of nanostructured ferritic alloys to high-dose heavy ion irradiation, Journal of Nuclear Materials, 445 (2014) 251-260.

[5] C.M. Parish, M.K. Miller, Aberration-Corrected X-Ray Spectrum Imaging and Fresnel Contrast to Differentiate Nanoclusters and Cavities in Helium-Irradiated Alloy 14YWT, Microscopy and Microanalysis, 20 (2014) 613-626.